Power Electronic Systems
Laboratory

Proceedings of the 16th Annual IEEE Energy Conversion Congress and Exposition (ECCE 2024), Phoenix, AZ, USA, October 20-24, 2024

Single-Stage Isolated Bidirectional Extended-Functionality X-Rectifier for EV Chargers with Three/Single-Phase AC Input Capability

D. Zhang,
S. Weihe,
J. Huber,
J. W. Kolar

ETH zürich

Single-Stage Isolated Bidirectional Extended-Functionality X-Rectifier for EV Chargers with Three/Single-Phase AC Input Capability

Daifei Zhang, Sven Weihe, Jonas Huber, and Johann W. Kolar
Power Electronic Systems Laboratory, ETH Zurich, Switzerland

***Abstract*—This paper introduces a novel single-stage isolated eXtended-functionality rectifier (X-Rectifier) designed to meet key requirements for next-generation electric vehicle (EV) on-board chargers (OBCs): Operation with the same nominal power in both, three-phase (3-Φ) and single-phase (1-Φ) grid connection, and bidirectional, fully decoupled power flow regulation in all three grid phases. The circuit structure facilitates the use of novel 600 V monolithic bidirectional GaN transistors when interfacing a 400 V (line-to-line rms, 565 V peak) grid, reducing hardware complexity. The paper first explains the operating principle of the X-Rectifier using equivalent circuits and then discusses a proof-of-concept modulation method applicable to both, operations in 3-Φ and 1-Φ grids. Detailed circuit simulations verify the X-Rectifier's extended functionality like 3-Φ grid-forming/standalone operation under extreme load imbalance (i.e., with only one phase loaded), and highlight potential performance improvements through alternative/advanced modulation schemes.**

***Index Terms*—Single-Stage, Galvanically Isolated, Bidirectional, Extended-Functionality Rectifier, On-Board Charger (OBC).**

I. Introduction

On-board chargers (OBCs) in electric vehicles (EVs) are typically required to provide galvanic isolation and bidirectional power flow between a battery and a three-phase (3-Φ) or a split-phase/single-phase (1-Φ) grid depending on the charging location as shown in **Fig. 1**, whereby in both cases the same nominal power should be achieved, and a wide battery voltage range (e.g., 200 V to 450 V) should be supported [1]–[11]. With future smart-grid/smart-home concepts, EVs also take a central role as energy hubs, providing grid support (vehicle-to-grid, V2G) or grid-forming/islanding capability for homes (vehicle-to-home, V2H), and could act as standalone three/single-phase power sources, e.g., on construction sites. Thus, next-generation OBCs should not only facilitate bidirectional power flow in standard grid-following operation, but also enable fully independent regulation of individual phase currents and/or voltages in both grid-supporting or grid-forming/standalone mode [12].

Whereas state-of-the-art OBCs are typically two-stage systems (consisting of an ac-dc rectifier and a cascaded isolated dc-dc converter), single-stage isolated ac-dc converters have been extensively analyzed for their potential to achieve higher conversion efficiency with lower implementation effort [13], [15]–[19]. Compared to matrix-type single-stage isolated converters [20], phase-modular topologies can interface a 1-Φ grid with the same nominal power as in the 3-Φ case without significant additional component stress. Such phase-modular single-stage isolated ac-dc converter topologies can be derived from 3-Φ dual active bridge (DAB) dc-dc converters [21]–[23] by replacing the dc-input front-end (converting a dc voltage to a high-frequency three-phase voltage applied to the transformer) with an ac-input front-end (directly converting a low-frequency three-phase mains voltage system to a high-frequency three-phase voltage applied to the transformer) as

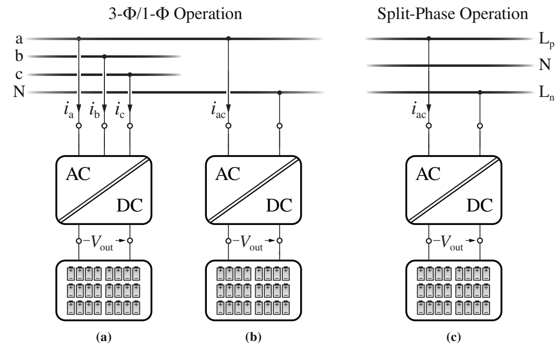

Fig. 1: Block diagram of a galvanically isolated single-stage ac-dc EV on-board charger (OBC) connected to **(a)** a three-phase (3-Φ), **(b)** a single-phase (1-Φ), or **(c)** a split-phase grid. In all three scenarios, the next-generation OBC must support the same nominal power flow in both directions.

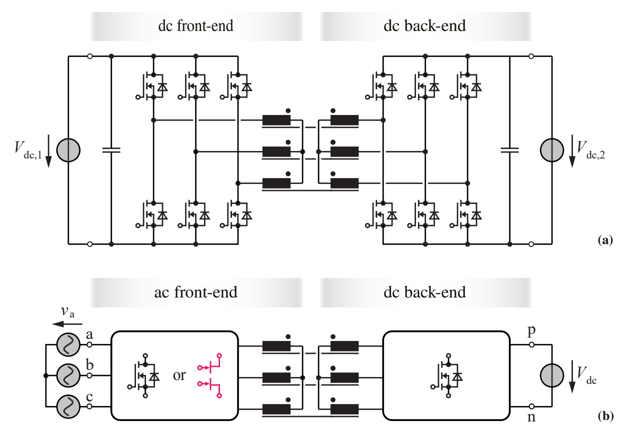

Fig. 2: Derivation of single-stage isolated ac-dc rectifier topologies from **(a)** the well-known 3-Φ dual active bridge (DAB) dc-dc converter by **(b)** replacing the dc-ac front-end by an ac-ac front-end directly converting the low-frequency 3-Φ mains voltage system into a high-frequency 3-Φ voltage system applied to the primary-side transformer terminals. **Fig. 3** shows specific realizations employing either conventional unidirectional switches or novel monolithic bidirectional switches (BDSs) in the ac front-ends.

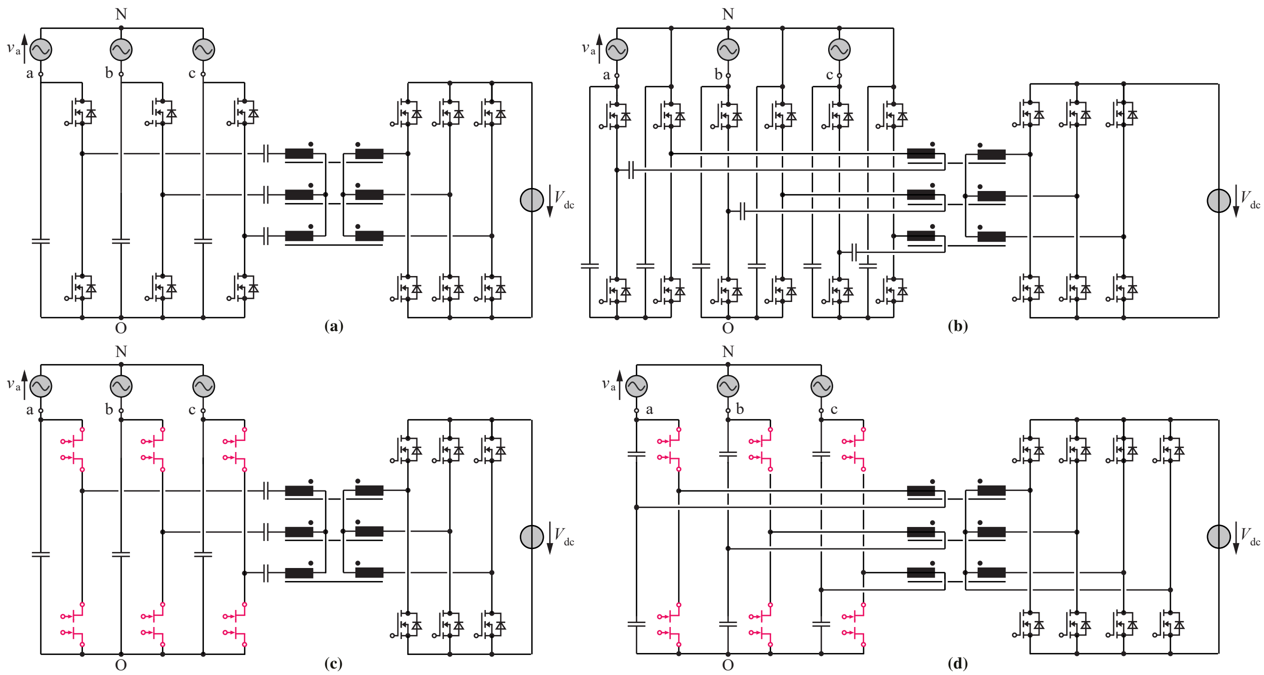

Fig. 3: Phase-modular single-stage isolated 3-Φ ac-dc converters (see **Fig. 2b**) discussed in recent literature. The ac-side front-end of **(a)** employs standard power transistors but requires a dc-offset of the input capacitor voltages and hence 900 V devices are needed [13], whereas **(b)** uses a cycloconverter approach where 650 V devices suffice to block the phase voltage amplitude (325 V in a 400 V line-to-line rms grid); on the other hand twelve instead of six power transistors are necessary [14]. Alternatively, recently available 650 V GaN monolithic BDSs enable direct ac-ac conversion with again only six power transistors as shown in **(c)** [14] and **(d)** [15].

indicated in **Fig. 2**. The operating principle of such DAB-type single-stage isolated three-phase ac-dc converters has been comprehensively explained in [16], where, however, a circuit topology without phase modularity and/or decoupled phases has been considered.

Fig. 3 shows four topology variants of phase-modular single-stage isolated three-phase ac-dc converters, which have been published in the recent literature [13]–[15]. The topology from **Fig. 3a** employs unidirectional power transistors in the ac frond-end, and to prevent short-circuits through reverse-conducting diodes, the input capacitor voltages must remain positive at all times. This is achieved by maintaining a positive offset voltage between potentials N and O (in the most simple case, a constant offset voltage). However. this approach requires the transistors to block a maximum voltage equal to twice the grid phase voltage amplitude (e.g., 650 V for a 400 V line-to-line rms grid), which typically necessitates at least 900 V transistors [13]. The variant from **Fig. 3b** addresses the high blocking voltage requirement by using three single-phase cycloconverters in the ac front-end. This approach reduces the transistor voltage stress to the phase voltage amplitude, i.e., to 325 V. Hence, 650 V/650 V transistors suffice, but the topology requires an increased number of devices (12 instead of 6 in the front-end) [14]. Alternatively, recently available 650 V GaN monolithic bidirectional switches (BDSs) could be employed to simplify the circuit structure of the cycloconverter and to reduce the component count as shown in **Fig. 3c** [14]. Compared to the topology from **Fig. 3a**, the control is simplified as there is no need for an offset voltage injection and regulation. Finally, **Fig. 3d** shows a topology with full phase modularity of the ac front-end [15], i.e., the primary-side transformer windings are not coupled via a common star point as in **Fig. 3c**. Note further a fourth bridge-leg is implemented in the dc back-end and connected to the star point formed by the secondary-side transformer windings, thus also creating phase-modularity on the secondary side.

Drawing from the BDS-based topologies discussed above, this paper introduces a new phase-modular single-stage isolated ac-dc converter with eXtended-functionality (X-Rectifier, see **Fig. 4**) that meets all requirements for next-generation OBCs: Single-stage power conversion, galvanic isolation, 3-Φ and 1-Φ operation, and bidirectional, decoupled power flow regulation in all three grid phases. The proposed X-Rectifier interfaces the grid with a phase-modular Y-connected (star point O in **Fig. 4**) arrangement of half-bridges equipped with BDSs. The blocking voltage is defined by the phase voltage amplitude (and not by the line-to-line voltage amplitude, as, e.g., in matrix-type circuits [20]), for interfacing both, a 3-Φ or a 1-Φ grid. Therefore, latest-generation 650 V monolithic GaN BDSs are applicable for interfacing a 400 V (line-to-line rms) grid.

A key distinguishing feature of the X-Rectifier is the connection between the the ac front-end star point O and the star point Y formed by the primary-side windings of the HF transformer[1] This connection, together with the open-delta

[1]Three individual HF transformers or a magnetically integrated three-phase transformer might be used.

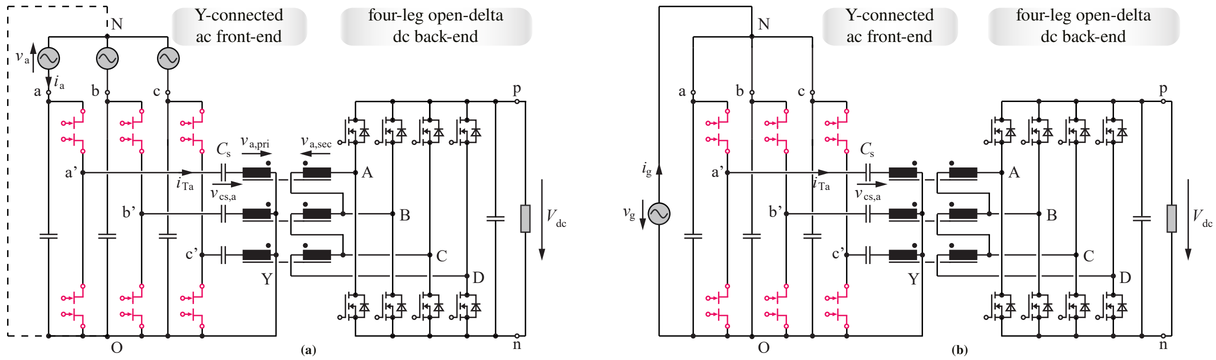

Fig. 4: Power circuit of the proposed single-stage isolated ac-dc converter, the eXtended-functionality rectifier (X-Rectifier), delivering the same nominal power in **(a)** a 3-Φ and **(b)** a 1-Φ grid. Fully independent power flow regulation in the three grid phases is enabled by the connection between the primary-side transformer star point Y and the front-end star point O, and by the open-delta winding configuration with a four-leg switching stage on the secondary side. The capacitors C_s connected in series with the primary windings of the transformer are sized to block the LF, i.e., 50 Hz, voltage components and/or to avoid saturation of the compact HF transformer.

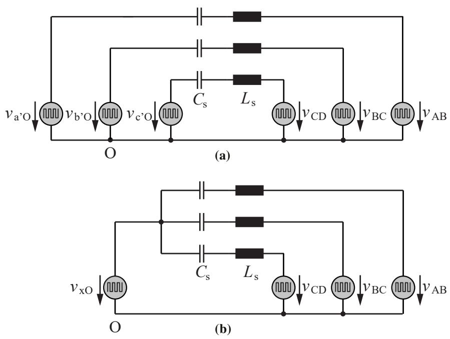

Fig. 5: Equivalent circuit of the X-Rectifier when operating in **(a)** a 3-Φ and **(b)** a 1-Φ grid. The labels of the equivalent voltage sources refer to nodes of the full circuit in **Fig. 4**. The LF-blocking capacitors C_s are transparent at the switching frequency and hence the system can be treated like three independent dual active bridge (DAB) converters with series inductances L_s.

configuration of the transformer's secondary-side windings connected to a four-leg switching stage, enables decoupled regulation of the power flows in the three transformer windings and, consequently, in the three grid phases.

In the following, first **Section II** explains the operating principle of the X-Rectifier for 3-Φ and 1-Φ connection and introduces a low-complexity proof-of-concept modulation scheme. **Section III** then employs detailed circuit simulations to verify 3-Φ and 1-Φ operation with both power flow directions, and the extended functionality is demonstrated by considering operation from an asymmetric three-phase grid, as well as standalone grid-forming operation, where the battery supplies a heavily unbalanced ac-side load. Finally, **Section IV** briefly compares open-delta and wye configurations of the secondary-side transformer windings before **Section V** concludes the paper.

II. Operating Principle of X-Rectfier

This section discusses the operating principle of the X-rectifier (see **Fig. 4**) and, aiming at highlighting the X-Rectifier topology's capability to provide the extended functionality required of future OBCs, introduces a proof-of-concept modulation method that enables operation in 3-Φ (symmetric and asymmetric) and 1-Φ grids as well as grid-forming/standalone operation without requiring modifications of the modulator nor mode switching.

A. Equivalent Circuits and Basic Considerations

The proposed X-Rectifier topology shown in **Fig. 4** is derived from the circuit shown in **Fig. 3c** through two key modifications:

- A connection of the ac front-end star point O and the star point Y of the primary-side transformer windings enables independent definition of each primary transformer voltage, each of which solely depends on the corresponding input capacitor voltage and the bridge-leg switching state.
- The open-delta configuration of the secondary-side transformer windings toghether with a four-leg switching stage enables independent definition of the three secondary-side transformer winding voltages (with certain restrictions briefly discussed below).

To facilitate the analysis and explanation of the modulation, **Fig. 5a** shows an equivalent circuit for interfacing with a 3-Φ grid (see **Fig. 4a**), where the three bridge-legs of the front-end are replaced by three switched voltage sources referenced to the potential O, e.g., $v_{a'O}$. These primary-side switched voltage sources are connected in series with the LF-blocking capacitors C_s, the transformer leakage inductances L_s, and three further switched voltage sources that represent the secondary-side transformer winding voltages (referred to the primary-side according to the transformer turns ratio). These secondary-side switched voltages are defined by the difference between the switch-node voltages of two adjacent bridge-legs, e.g., the switching states of legs A and B define v_{AB}. Since in each phase the voltage applied to the series impedance is fully defined by the two switched voltage sources, all can be referred to a common potential O.

As indicated in **Fig. 4b**, interfacing a 1-Φ grid with nominal power is advantageously enabled by connecting the ac input terminals of the three ac front-end bridge-legs in parallel. Then, if all ac front-end bridge-legs are switched synchronously (details below), the equivalent circuit for 1-Φ operation can be simplified by using a single primary-side switched voltage source v_{xo} as shown in **Fig. 5b**. However, the back-end bridge-legs still need to be modulated independently to regulate the power transfer through each transformer winding and thus ensuring symmetric stress distribution. Therefore, the equivalent circuit of the dc back-end does not change.

The equivalent circuit clearly indicates that decoupled regulation of the power flows in the three phases is possible if all switched voltages can be arbitrarily selected, as the circuit essentially consists of three individual DAB converters.

However, the three secondary-side transformer winding voltages v_{AB}, v_{BC}, and v_{CD} are not fully independent if a four-leg back-end switching stage is used: As discussed in [24], it is possible to arbitrarily and independently select the duty cycle of each of these voltages, but then a certain phase relationship between the voltages results and cannot be changed. Consequently, a corresponding phase difference between the three primary-side transformer voltages would result even for a balanced system where all three phases are symmetrically loaded. As in any DAB converter, the power flow in each phase can then be adapted by further modifying the phase shift between the corresponding primary-side and secondary-side transformer voltages. This approach has been employed in [24] to a multi-port dc-dc converter and in [15] to the ac-dc rectifier topology shown in **Fig. 3d**.

Here, aiming at primarily highlighting the X-Rectifier topology's capability to provide the extended functionality required of future OBCs, we employ an alternative low-complexity proof-of-concept modulation that is based on retaining the synchronous switching operation of the ac front-end bridge-legs as in [13], [14], [16], and supports operation in 3-Φ (symmetric and asymmetric) and 1-Φ grids using the same calculation method for the duty cycles of the secondary-side four-leg switching stage. This is discussed in the following and illustrated by simulation results for (symmetric) 3-Φ and 1-Φ operation (see **Fig. 6**) considering the exemplary specifications listed in **Tab. I**.

B. AC Front-End Modulation

The three bridge-legs of the ac front-end are always pulse-width modulated (PWM) synchronously with a fixed duty cycle of 50%. Each switching period (see zoomed views in **Fig. 6**) begins with a positive half-cycle where the high-side switches of the three bridge-legs are on for half of the switching period. Taking phase a as an example, the switch node voltage $v_{\mathrm{a'O}}$ equals the phase voltage v_{a}. During the second half, i.e., a negative half-cycle, the low-side switches of the three bridge-legs are on, and the switch node voltage $v_{\mathrm{a'O}}$ equals 0 V. Consequently, the switch node voltage $v_{\mathrm{a'O}}$ toggles between 0 V and the phase voltage v_{a}, and contains both, a low-frequency (LF, i.e., grid frequency of 50 Hz) component with an amplitude of $v_{\mathrm{a}}/2$, and HF (switching frequency) components. The capacitor C_{s} then forms a frequency-dependent voltage divider with the transformer leakage inductance L_{s} (see **Fig. 5**) such that C_{s} blocks the LF voltage $v_{\mathrm{cs,a}} = v_{\mathrm{a}}/2$ and thus prevents

TABLE I: Specifications considered for the circuit simulations.

	Description	Value
V_{in}	RMS grid phase volt.	230 V
V_{out}	DC output volt.	400 V
P_{out}	Rated output power	6.6 kW
f_{sw}	Sw. frequency	150 kHz
$N_{\mathrm{p}} : N_{\mathrm{s}}$	Turns ratio	8:6
L_{s}	Leakage inductance	8 µH
C_{s}	Series Capacitance	10 µF

transformer saturation. Finally, only an amplitude-modulated HF voltage with amplitude

$$v_{\mathrm{a,pri}} = v_{\mathrm{a'N}} - v_{\mathrm{cs,a}} = v_{\mathrm{a'N}} - v_{\mathrm{a}}/2 = v_{\mathrm{a}}/2 \tag{1}$$

is applied to the primary-side transformer winding, see **Fig. 6**.

C. DC Back-End Modulation

To achieve DAB-type operation as in [13], [14], [16], the modulation of the secondary-side should essentially ensure that in each switching half-period, the voltage-time area applied to a secondary-side winding equals that applied to the corresponding primary-side winding (taking into account the transformer turns ratio). This is achieved by adjusting the duty cycle of each secondary-side transformer voltage according to the associated primary-side voltage amplitude. As here the primary-side bridge-legs switch synchronously, there should also be no phase-shift between the three secondary-side transformer voltages, i.e., just a single PWM carrier for all four bridge-legs can be employed. As in any DAB-type converter, the power flow is then regulated via the phase shift φ (identical for all three phases) between the primary-side and the secondary-side HF voltages.

1) 3-Φ Operation

On the secondary-side of the transformer with its open-delta winding configuration, the voltage applied to each winding is the difference between the switch-node voltages of two adjacent bridge-legs (e.g., v_{AB}). Taking the first positive half-cycle as an example, the DM duty cycles for the four bridge-legs are

$$\begin{aligned} d'_{\mathrm{pA}} &= (v_{\mathrm{a}} - v_{\mathrm{c}} + 3 \cdot v_{\mathrm{pAsy}}) \cdot K_{\mathrm{v}}, \\ d'_{\mathrm{pB}} &= (v_{\mathrm{b}} - v_{\mathrm{a}} + 2 \cdot v_{\mathrm{pAsy}}) \cdot K_{\mathrm{v}}, \\ d'_{\mathrm{pC}} &= (v_{\mathrm{c}} - v_{\mathrm{b}} + v_{\mathrm{pAsy}}) \cdot K_{\mathrm{v}}, \\ d'_{\mathrm{pD}} &= (v_{\mathrm{a}} - v_{\mathrm{c}}) \cdot K_{\mathrm{v}}, \end{aligned} \tag{2}$$

with $v_{\mathrm{pAsy}} = v_{\mathrm{a}} + v_{\mathrm{b}} + v_{\mathrm{c}}$ and $K_{\mathrm{v}} = N_{\mathrm{s}}/6N_{\mathrm{p}}V_{\mathrm{dc}}$; V_{dc} is the dc output voltage and $N_{\mathrm{p}}/N_{\mathrm{s}}$ is the transformer turns ratio. Considering phase a as an example, the effective duty cycle of the rectangular voltage applied to the secondary-side winding, i.e., v_{AB} in **Fig. 5**, is

$$\begin{aligned} d_{\mathrm{a}} &= (d'_{\mathrm{pA}} - d'_{\mathrm{pB}}) \\ &= (2v_{\mathrm{a}} - v_{\mathrm{b}} - v_{\mathrm{c}} + v_{\mathrm{pAsy}}) \cdot N_{\mathrm{s}}/6N_{\mathrm{p}}V_{\mathrm{dc}} \\ &= 3v_{\mathrm{a}} \cdot N_{\mathrm{s}}/6N_{\mathrm{p}}V_{\mathrm{dc}} = v_{\mathrm{a}}/2 \cdot 1/V_{\mathrm{dc}} \cdot N_{\mathrm{s}}/N_{\mathrm{p}}, \end{aligned} \tag{3}$$

i.e., $d_{\mathrm{a}} \propto v_{\mathrm{a}}$as required.

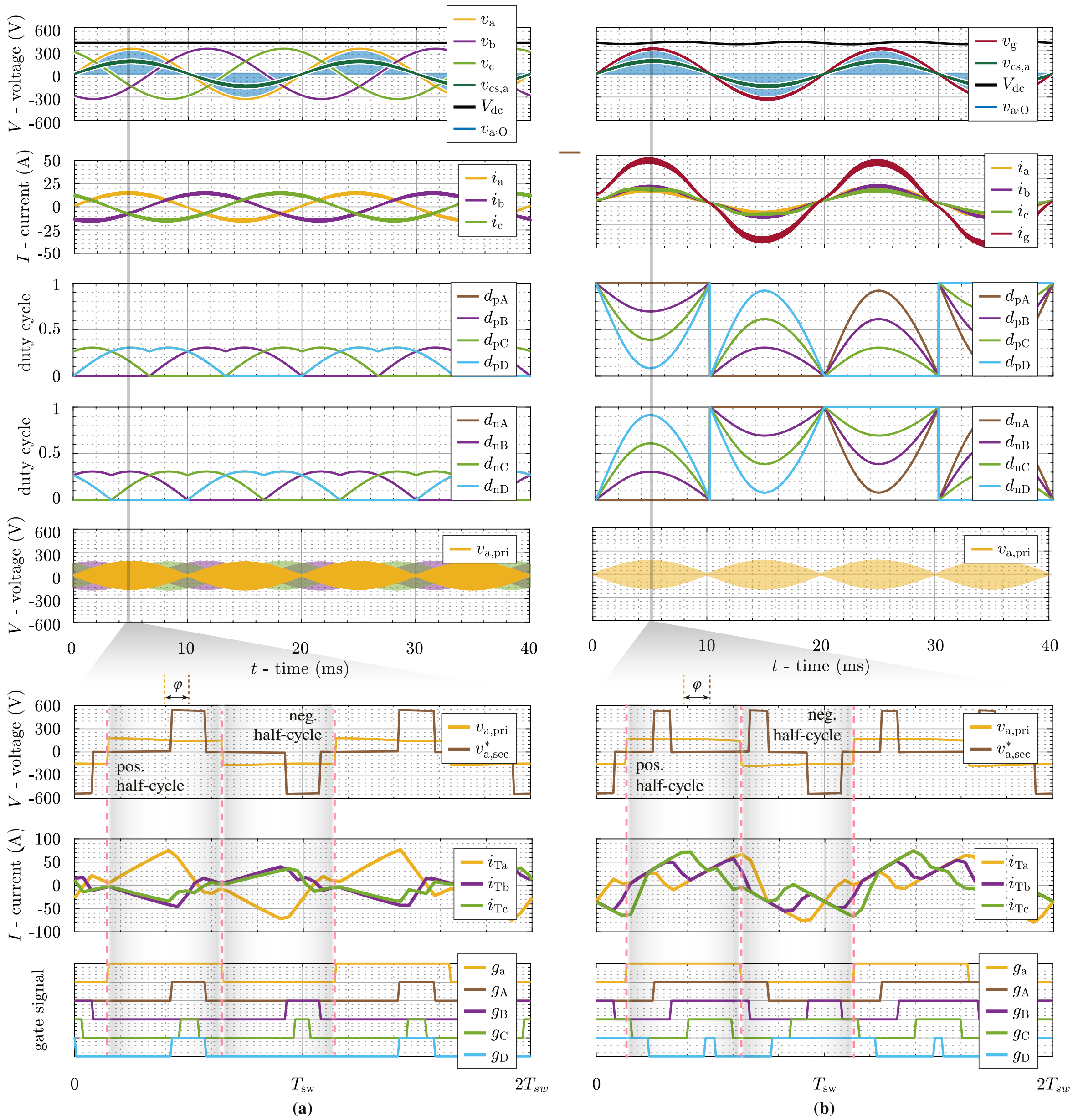

Fig. 6: Simulated key waveforms of the proposed X-Rectifier for charging operation from **(a)** a 3-Φ grid (see **Fig. 4a**) and **(b)** a 1-Φ grid (see **Fig. 4b**), delivering nominal power (6.6 kW) to the dc output (400 V) in both cases. The three bridge-legs of the ac front-end are always pulse-width modulated (PWM) synchronously with a fixed duty cycle of 50%. The four bridge-legs of the dc back end are operated with the proof-of-concept modulation method introduced in **Section II**. The zoomed views show exemplary transformer voltage and current waveforms as well as gate signals over two switching periods.

Note that if the 3-Φ grid voltages are symmetric, the asymmetric correction voltage $v_{\mathrm{pAsy}} = v_{\mathrm{a}} + v_{\mathrm{b}} + v_{\mathrm{c}} = 0$ and $d'_{\mathrm{pA}} = d'_{\mathrm{pD}}$. Thus, the four-leg back-end operates as a conventional 3-Φ three-leg delta-type rectifier [25]. In the cases with asymmetric 3-Φ grid voltages, $v_{\mathrm{pAsy}} \neq 0$ becomes effective, resulting in different values for d'_{pA} and d'_{pD}. Consequently, all four bridge-legs operate with different duty cycles as discussed later in **Section III**.

Furthermore, a CM duty cycle must be selected to ensure that all four duty cycles of the switch-node voltages remain non-negative at any given time. E.g., a CM duty cycle

$$d_{\mathrm{pCM}} = -\min(d'_{\mathrm{pA}}, d'_{\mathrm{pB}}, d'_{\mathrm{pC}}, d'_{\mathrm{pD}},) \tag{4}$$

is added to the DM duty cycles, resulting in

$$\begin{aligned} d_{\mathrm{pA}} &= d'_{\mathrm{pA}} + d_{\mathrm{pCM}}, \quad d_{\mathrm{pB}} = d'_{\mathrm{pB}} + d_{\mathrm{pCM}}, \\ d_{\mathrm{pC}} &= d'_{\mathrm{pC}} + d_{\mathrm{pCM}}, \quad d_{\mathrm{pD}} = d'_{\mathrm{pD}} + d_{\mathrm{pCM}}. \end{aligned} \tag{5}$$

Advantageously, the bridge-leg with the minimum DM duty cycle is always clamped as indicated in **Fig. 6a**, thereby avoiding switching losses. The injected CM duty cycle could be further optimized for various control purposes, e.g., more evenly distributing conduction and switching losses among the transistors.

For the negative half-cycle, the polarities of the three primary-side transformer voltages are reversed, resulting in the DM duty cycles for the four bridge-legs as

$$\begin{aligned} d'_{\mathrm{nA}} &= (-v_{\mathrm{a}} + v_{\mathrm{c}} + 3 \cdot v_{\mathrm{nAsy}}) \cdot K_{\mathrm{v}}, \\ d'_{\mathrm{nB}} &= (-v_{\mathrm{b}} + v_{\mathrm{a}} + 2 \cdot v_{\mathrm{nAsy}}) \cdot K_{\mathrm{v}}, \\ d'_{\mathrm{nC}} &= (-v_{\mathrm{c}} + v_{\mathrm{b}} + v_{\mathrm{nAsy}}) \cdot K_{\mathrm{v}}, \\ d'_{\mathrm{nD}} &= (-v_{\mathrm{a}} + v_{\mathrm{c}}) \cdot K_{\mathrm{v}}, \end{aligned} \tag{6}$$

with $v_{\mathrm{nAsy}} = -v_{\mathrm{a}} - v_{\mathrm{b}} - v_{\mathrm{c}}$. Note that reversing the polarities of all three phase voltages is equivalent to a 180° phase shift of the DM duty cycles in time, as shown in **Fig. 6a**.

Fig. 6a shows simulation results of the X-Rectifier in charging operation from a symmetric 3-Φ grid with nominal load of 6.6 kW. The output voltage is controlled to the nominal value of 400 V via the phase shift φ between the primary-side and the secondary-side carrier signal, and the difference between the voltages applied to the primary-side and secondary-side transformer windings leads to triangular currents in the leakage inductances. Note that, as in [13], [14], [16], the employed modulation method directly achieves sinusoidal mains currents without any further underlying control loops (even though these could be added to improve the mains current quality, etc.).

2) 1-Φ Operation

The duty cycle calculation method described above for the 3-Φ case is directly applicable to 1-Φ operation of the X-Rectifier. Considering the positive half-cycle, $v_{\mathrm{a}} = v_{\mathrm{b}} = v_{\mathrm{c}} = v_{\mathrm{g}}$,

$$v_{\mathrm{pAsy}} = v_{\mathrm{a}} + v_{\mathrm{b}} + v_{\mathrm{c}} = 3v_{\mathrm{g}}, \tag{7}$$

and the DM duty cycles are

$$\begin{aligned} d'_{\mathrm{pA}} &= (v_{\mathrm{a}} - v_{\mathrm{c}} + 3 \cdot v_{\mathrm{pAsy}}) \cdot K_{\mathrm{v}} &&= 9v_{\mathrm{g}} \cdot K_{\mathrm{v}}, \\ d'_{\mathrm{pB}} &= (v_{\mathrm{b}} - v_{\mathrm{a}} + 2 \cdot v_{\mathrm{pAsy}}) \cdot K_{\mathrm{v}} &&= 6v_{\mathrm{g}} \cdot K_{\mathrm{v}}, \\ d'_{\mathrm{pC}} &= (v_{\mathrm{c}} - v_{\mathrm{b}} + v_{\mathrm{pAsy}}) \cdot K_{\mathrm{v}} &&= 3v_{\mathrm{g}} \cdot K_{\mathrm{v}}, \\ d'_{\mathrm{pD}} &= (v_{\mathrm{a}} - v_{\mathrm{c}}) \cdot K_{\mathrm{v}} &&= 0. \end{aligned} \tag{8}$$

Since $v_{\mathrm{a}} = v_{\mathrm{b}} = v_{\mathrm{c}} = v_{\mathrm{g}}$, the asymmetric correction voltages v_{pAsy} and v_{nAsy} determine the duty cycles. Thus, the effective duty cycle of the rectangular voltage applied to the secondary-side winding, i.e., v_{AB} in **Fig. 5**, is again

$$d_{\mathrm{a}} = (d'_{\mathrm{pA}} - d'_{\mathrm{pB}}) = 3v_{\mathrm{g}} \cdot K_{\mathrm{v}} = {}^{v_{\mathrm{a}}}\!/_{2} \cdot {}^{1}\!/_{V_{\mathrm{dc}}} \cdot {}^{N_{\mathrm{s}}}\!/_{N_{\mathrm{p}}}, \tag{9}$$

which again ensures balanced voltage-time areas on the primary-side and secondary-side of the transformer. The duty cycle calculation for the negative half-cycle follows the same process as for the 3-Φ case and is therefore not repeated here.

Fig. 6b presents according simulation results for charging operation of the X-Rectifier from a 1-Φ grid with the same nominal power of 6.6 kW. The three bridge-legs of the ac front-end operate in parallel (see **Fig. 4b**) and are still modulated synchronously with a 50% duty cycle. This configuration allows for the nominal output power to be achieved without increasing the front-end transistor current stresses compared to 3-Φ operation. Again, the output voltage is controlled to the nominal value of 400 V via the phase shift φ. This modulation then ensures approximately equal power transfer through all three transformers (note the similar HF transformer currents as well as equal LF input phase currents $i_{\mathrm{a}} \approx i_{\mathrm{b}} \approx i_{\mathrm{c}} \approx i_{\mathrm{g}}/3$).

The selection of the CM duty cycle is a degree of freedom, as the power transfer depends solely on the duty cycle differences between the back-end bridge-legs, not the absolute duty cycles. Specifically, the order of the DM duty cycles from (9) must be maintained, but a CM offset can be selected to either clamp the lowest value to 0 or the highest value to 1, which is demonstrated in the simulation: During the first 20 ms, the duty cycle of bridge-leg *A* is either 0 (low-side transistor is permanently on) or 1 (high-side transistor is permanently on) to avoid switching losses. In the second 20 ms (20 ms to 40 ms), bridge-leg *D* is clamped instead of bridge-leg *A* to minimize switching losses (note that it is not possible to clamp legs B or C). Alternating the clamping phase helps balance the current stress among the three phases of the ac front-end.

III. Extended Functionality

Whereas the simulation results shown in **Fig. 6** cover the standard cases of drawing power from either a symmetric 3-Φ or a 1-Φ grid to charge a battery, this section provides further simulation results that confirm the X-Rectifier's extended functionality, i.e., the capability to operate from a asymmetric 3-Φ grid, and to act in 3-Φ grid-forming/standalone mode with extremely asymmetric phase loading. The proof-of-concept modulation method introduced in **Section II** facilitates both.

A. Charging from an Asymmetric 3-Φ Grid

Fig. 7a presents the charging operation from a 3-Φ grid with asymmetric phase voltages, where phase *a* has a reduced amplitude (50%). Again, the output voltage is controlled to a constant nominal value of 400 V via the phase shift φ, and nominal load is supplied. The modulation introduced in **Section II** ensures that the phase currents are proportional to the respective phase voltage. In particular, the phase current i_{a} drawn from phase *a* is reduced. However, as the output voltage is still regulated to a constant value and hence the output power is kept constant, too, the current drawn by the other two phases increases (this is, of course, only possible within certain limits given by the component stresses) and a certain low-frequency distortion of the phase currents results.

B. 3-Φ Grid-Supporting/Standalone Operation

Finally, **Fig. 7b** shows 3-Φ grid-forming/standalone operation, where the X-Rectifier provides a symmetric 3-Φ voltage system at the ac terminals from a 400 V battery. Especially in standalone operation, e.g., if the vehicle acts as a power source on a construction side, the 3-Φ loads can be heavily unbalanced (i.e., certain loads connect only to one of the phases). The simulation considers an extreme scenario where only phase a is loaded, while no loads are connected to phases b and c. Whereas still a single phase shift φ between the carriers of the front-end and of the back-end converter stages is used, which can be pre-calculated, e.g., based on the average power to be transferred, three PI controllers are used to track the phase voltage references across the input capacitors employing the controller outputs (instead of the measured phase voltages

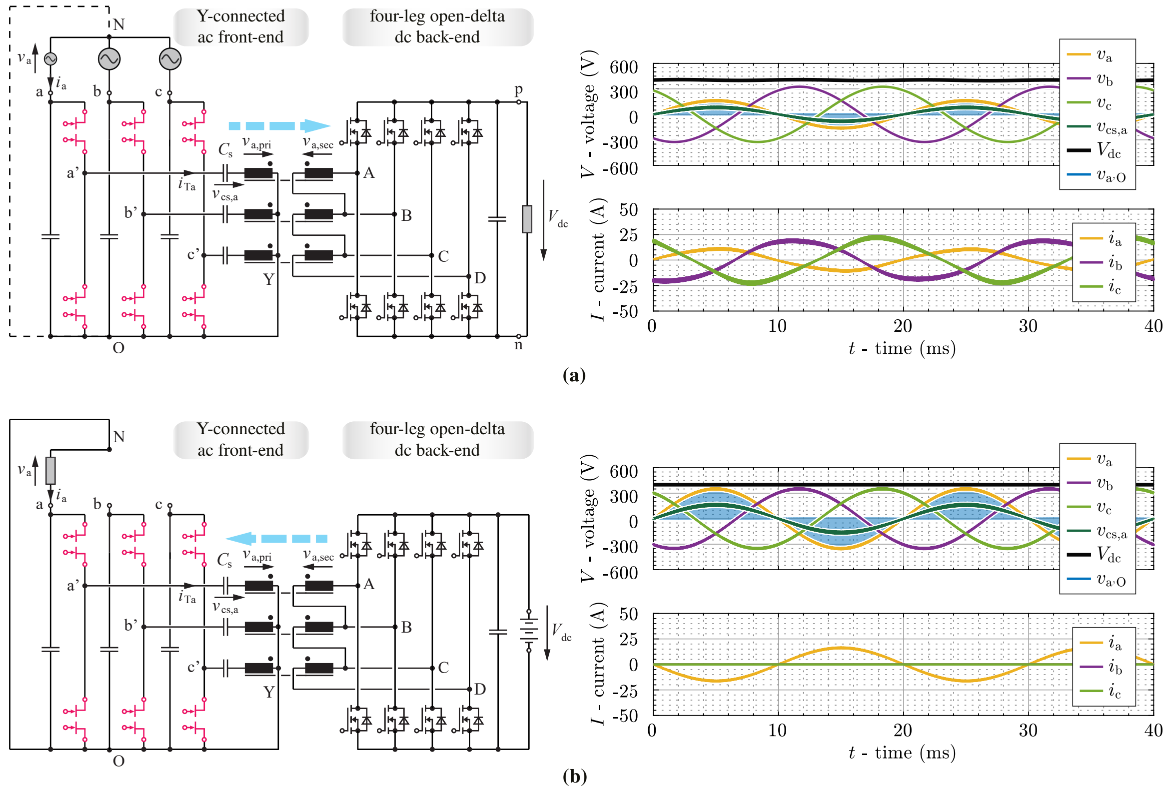

Fig. 7: Simulated key waveforms of the proposed X-Rectifier for **(a)** charging operation from an unbalanced 3-Φ grid (phase voltage v_a reduced to 50%), where i_a is reduced accordingly (to maintain constant output power, the other two phase currents are increased and show certain distortions in this example), and **(b)** for grid-forming/standalone operation where a symmetric 3-Φ voltage system is provided at the ac terminals, only one of which (here phase a) is loaded, i.e., no load is connected to phases b and c).

v_a, v_b, v_c) in the calculation of the secondary-side DM duty cycles with (2)…(5). The simulation results demonstrate that the X-Rectifier topology can provide a symmetric 3-Φ voltage system at the ac terminals despite highly asymmetric loading of the phases, i.e., facilitates decoupled power flow regulation in the three phases.

IV. Transformer Configuration & Current Stress

To provide four terminals for interfacing a four-leg switching stage, the secondary-side transformer windings can be configured either in a star configuration with the star point forming the fourth terminal (see **Fig. 3d**) or in an open-delta configuration (see **Fig. 4**). It is thus interesting to briefly consider the current stresses of the four bridge-legs during 3-Φ and 1-Φ operation with the proof-of-concept modulation from **Section II**.

Considering first the open-delta configuration and 3-Φ operation, specifically a representative 60° interval of the grid period during which $v_a > 0$ and $v_b, v_c < 0$, **Fig. 8a** qualitatively indicates the resulting transformer winding and terminal currents during the positive half-cycle of the switching period (i.e., when all high-side switches of the primary-side bridge-legs are on, also see **Fig. 6**). Power transfer from the ac to the dc side then requires primary currents flowing into node a' and out of nodes b' and c', which are further (roughly) proportional to the respective phase voltages. This directly defines the direction and magnitude of the secondary-side winding currents, and the secondary-side terminal currents follow from Kirchhoff's current law. In particular, note that the currents in terminals A and D are directly given by the winding currents, whereas the currents in the terminals B and C are defined by *two* winding currents, which here leads to high current stress for bridge-leg B and very low current stress for bridge-leg C.

In the case of 1-Φ charging operation, the currents flowing through the three transformer windings always share the same direction and have similar magnitudes. As a result, the currents flowing through terminals B and C—obtained from the differences between the currents of the two connected transformer windings—are relatively small. Notably, the current sharing among the four bridge-legs is more balanced; no single terminal is heavily loaded, unlike terminal B in the 3-Φ case.

In the alternative star configuration shown in **Fig. 8b**, the current in the terminals A, B, and C are directly given by the corresponding primary-side currents and hence proportional to the corresponding phase voltage; the stresses of these three bridge-legs are thus similar for both, 3-Φ and 1-Φ operation. However, whereas there is zero current (ideally) through terminal D in 3-Φ operation if terminal Y is not connected, in 1-Φ operation, all three transformer winding currents flow in the same direction and are thus summed at terminal D, leading to excessive current stress of the corresponding bridge-leg.

Note that the above discussion is specific to the proof-

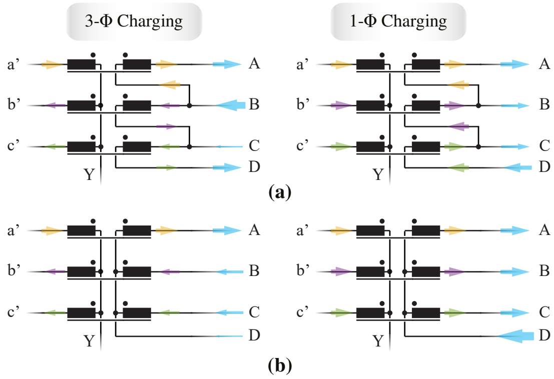

Fig. 8: Qualitative transformer winding and secondary-side terminal current stress for 3-Φ and 1-Φ charging mode using **(a)** an open-delta configuration as in **Fig. 4** or **(b)** a star configuration with the star point connected to terminal D as in **Fig. 3d**. The size of the arrow indicates the rms current value. For the open-delta case (a), high current stress appears in the middle two bridge-legs, e.g., terminal B, during 3-Φ operation. In contrast, the star configuration (b) leads to high current stress of bridge-leg D in 1-Φ operation. Note that the low-complexity modulation scheme employed in this paper for a basic proof-of-concept of the proposed converter topology could be optimized considering the transformer and power semiconductor component stresses with significant potential for improvement.

of-concept modulation method used throughout the paper; the proposed circuit topology leaves ample room for advanced/optimized modulation techniques and/or advanced/alternative transformer configurations that potentially enable significant performance improvements.

V. Conclusion

This paper proposes a single-stage isolated eXtended-functionality rectifier (X-Rectifier) for future EV OBCs, which can employ 650 V GaN monolithic BDSs in the phase-modular ac front-end when interfacing a 400 V (line-to-line rms, 565 V peak) grid. Further, the circuit structure features a connection between the star point formed by the three ac front-end BDS bridge-legs and the star point formed by the three primary-side transformer windings. Together with an open-delta configuration of the secondary-side transformer windings and a four-leg dc back-end switching stage, fully decoupled power flow regulation in all three transformers and hence in the three grid phases becomes possible. Using a low-complexity proof-of-concept modulation method, the paper demonstrates that the X-Rectifier topology can not only draw the same nominal power from the 3-Φ and the 1-Φ grid without excessive component stresses, but can also operate with an asymmetric 3-Φ grid, and further can act in a grid-forming/standalone mode, creating a symmetric 3-Φ voltage system despite extremely asymmetric loading of the phases, e.g., for applications on a construction site. Further performance optimization by means of advanced/optimized modulation methods will be explored in the scope of future research.

References

[1] H. Wouters and W. Martinez, "Bidirectional on-board chargers for electric vehicles: State-of-the-art and future trends," *IEEE Trans. Power Electron.*, vol. 39, no. 1, pp. 693–716, 2023.

[2] S. Rivera, S. M. Goetz, S. Kouro, P. W. Lehn, M. Pathmanathan, P. Bauer, and R. A. Mastromauro, "Charging infrastructure and grid integration for electromobility," *Proc. IEEE*, vol. 111, no. 4, pp. 371–396, 2022.

[3] F. Jin, A. Nabih, T. Yuan, and Q. Li, "A high-efficiency high-density three-phase CLLC resonant converter with a universally derived three-phase integrated transformer for on-board charger application," *IEEE Trans. Power Electron.*, early access, 2024.

[4] B. P. Do, M. G. Geda, J. Yun, K. Kang, S. Lee, and S. Choi, "Single-phase and three-phase compatible single-stage OBC with 6-switches secondary side," in *Proc. 10th IEEE Int. Power Electron. Motion Control Conf. (IPEMC-ECCE Asia)*, Chengdu, China, July 2024.

[5] M. Vazzoler, T. Caldognetto, D. Biadene, A. Petucco, and P. Mattavelli, "Isolated active front-end with integrated bidirectional GaN switches for battery chargers," in *Proc. IEEE Appl. Power Electron. Conf. Expo. (APEC)*, Long Beach, CA, USA, May 2024.

[6] E. Martinez-Vera and P. Banuelos-Sanchez, "Review of bidirectional DC-DC converters and trends in control techniques for applications in electric vehicles," *IEEE Lat. Am. Trans.*, vol. 22, no. 2, pp. 144–155, 2024.

[7] R. Pradhan, S. B. Shah, M. I. Hassan, Z. Wang, and A. Emadi, "A 15 kW wide-input reconfigurable three-level DAB converter for on-board charging of 1.25 kV electric vehicle powertrains," *IEEE Trans. Transp. Electr.*, early access, 2024.

[8] D. Zhang, J. Huber, and J. W. Kolar, "A three-phase synergetically controlled buck-boost current DC-link EV charger," *IEEE Trans. Power Electron.*, vol. 38, no. 12, pp. 15 184–15 198, 2023.

[9] I. Verbytskyi, M. M. Nadeem, A. Blinov, E. L. Carvalho, A. Chub, and D. Vinnikov, "Dynamic reconfiguration for wide output voltage range isolated buck-boost PFC converter," in *Proc. 8th IEEE Southern Power Electron. Conf. (SPEC)*, Florianopolis, Brazil, 2023.

[10] Y. Shen, R. A. Ghaderloo, C. Singhabahu, R. Resalayyan, and A. Khaligh, "Design and modeling of a two-stage PV inverter for single phase and three phase applications," in *Proc. IEEE Energy Convers. Congr. Expo. (ECCE USA)*, Nashville, TN, USA, 2023.

[11] Y. Wu, J. Xu, T. B. Soeiro, P. Bauer, and Z. Qin, "Frequency design of three-phase active front-end converter with reduced filter in EV chargers," *IEEE Trans. Transp. Electr.*, 2024, early access.

[12] F. Zhao, T. Zhu, L. Harnefors, B. Fan, H. Wu, Z. Zhou, Y. Sun, and X. Wang, "Closed-form solutions for grid-forming converters: A design-oriented study," *IEEE Open J. Power Electron.*, vol. 5, pp. 186–200, 2024.

[13] D. Menzi, F. Krismer, T. Ohno, J. Huber, J. W. Kolar, and J. Everts, "Novel bidirectional single-stage isolated three-phase buck-boost PFC rectifier system," in *Proc. IEEE Appl. Power Electron. Conf. Expo. (APEC)*, Orlando, FL, USA, Mar. 2023.

[14] D. Menzi, J. W. Kolar, H. Sarnago, O. Lucia, and J. E. Huber, "New 600 V GaN single-stage isolated bidirectional 400 V input three-phase PFC rectifier," in *Proc. IEEE Energy Convers. Congr. Expo. (ECCE USA)*, Nashville, TN, USA, Oct 2023.

[15] J. E. Bosso, M. Llomplat, G. G. Oggier, and G. O. García, "Isolated bidirectional DC-to-three-phase AC converter for integration of renewable energy sources to electric grid," *IET Power Electron.*, vol. 12, no. 8, pp. 2058–2068, 2019.

[16] R. Baranwal, K. V. Iyer, K. Basu, G. F. Castelino, and N. Mohan, "A reduced switch count single-stage three-phase bidirectional rectifier with high-frequency isolation," *IEEE Trans. Power Electron.*, vol. 33, no. 11, 2018.

[17] J. Lee, H. Jeong, T. LE, and S. Choi, "Three-phase single-stage bidirectional CCM soft-switching AC–DC converter with minimum switch count," *IEEE Trans. Power Electron.*, vol. 38, no. 2, pp. 2052–2062, Feb. 2023.

[18] M. Zhang, H. Zou, Z. Chen, R. Yu, and A. Q. Huang, "A novel single-stage bidirectional isolated three-phase resonant mode AC-DC PFC converter," in *Proc. IEEE Energy Convers. Congr. Expo. (ECCE USA)*, Nashville, TN, USA, Oct 2023.

[19] Y. Xu, Z. Wang, Y. Shen, Z. Zou, and M. Liserre, "A VSC based isolated matrix-type AC/DC converter without bidirectional power switches," *IEEE Trans. Ind. Electron.*, vol. 70, no. 12, pp. 12 442–12 452, 2023.

[20] N. D. Weise, K. K. Mohapatra, and N. Mohan, "Universal utility interface for plug-in hybrid electric vehicles with vehicle-to-grid functionality," in *Proc. IEEE Power Energy Soc. (PES) General Meet.*, Minneapolis, MN, USA, Jul. 2010.

[21] R. W. De Doncker, D. M. Divan, M. H. Kheraluwala, "A three-phase soft-switched high-power-density DC/DC converter for high-power applications," *IEEE Trans. Ind. Appl.*, vol. 27, no. 1, pp. 63–73, 1991.

[22] N. Hou and J. Hu and D. Mou and Y. Zhang and Y. Li and R. W. De Doncker, "A simple DC-offset eliminating method of the series-inductance current for the DAB DC–DC converter," *IEEE Trans. Power Electron.*, vol. 38, no. 4, pp. 4224–4228, 2022.

[23] J.-S. Hong, J.-I. Ha, S. Cui, and J. Hu, "Topology and control of an enhanced dual-active bridge converter with inherent bipolar operation capability for LVDC distribution systems," *IEEE Trans. Power Electron.*, vol. 38, no. 10, pp. 12 774–12 789, 2023.

[24] T. Ohno, S. Mirić, T. Guillod, F. Krismer, J. Huber, and J. W. Kolar, "New triple-output quad-active-bridge DC/DC converter employing a four-leg inverter input stage," in *Proc. 26th Int. Conf. Electr. Machines Syst. (ICEMS)*, Zhuhai, China, Nov. 2023, pp. 3984–3991.

[25] R. Greul, S. D. Round, and J. W. Kolar, "The delta-rectifier: Analysis, control and operation," *IEEE Trans. Power Electron.*, vol. 21, no. 6, pp. 1637–1648, 2006.